Journal of The Electrochemical Society, **157** (4) A499-A507 (2010)
0013-4651/2010/157(4)/A499/9/$28.00 © The Electrochemical Society

Aging Mechanisms of $LiFePO_4$ Batteries Deduced by Electrochemical and Structural Analyses

Ping Liu,[a,*,z] John Wang,[a] Jocelyn Hicks-Garner,[a,*] Elena Sherman,[a] Souren Soukiazian,[a] Mark Verbrugge,[b,*] Harshad Tataria,[b,*] James Musser,[c] and Peter Finamore[c]

[a]*HRL Laboratories, LLC, Malibu, California 90265, USA*
[b]*General Motors Corporation, Warren, Michigan 48092, USA*
[c]*John Deere Southeast Engineering Center, Charlotte, North Carolina 28241, USA*

The performance loss of lithium-ion batteries with lithium iron phosphate positive chemistry was analyzed using electrochemical characterization techniques such as galvanostatic charge–discharge at different rates, ac impedance, and hybrid pulse power characterization measurements. Differentiation analysis of the discharge profiles as well as in situ reference electrode measurement revealed loss of lithium as well as degradation of the carbon negative; the cell capacity, however, was limited by the amount of active lithium. Destructive physical analyses and ex situ electrochemical analyses were performed at test completion on selected cells. While no change in positive morphology and performance was detected, significant cracking and delamination of the carbon negative was observed. In addition, X-ray diffraction analysis confirmed the changes in the crystal structure of the graphite during cycling. The degradation of the carbon negative is consistent with the observations from the electrochemical analysis. Ex situ electrochemical analysis confirmed that active lithium controlled cell capacity and its loss with cycling directly correlated with cell degradation. The relationship between carbon negative degradation and loss of active lithium is discussed in the context of a consistent overall mechanism.
 [DOI: 10.1149/1.3294790]

Manuscript submitted November 1, 2009; revised manuscript received December 17, 2009. Published March 10, 2010.

Lithium-ion batteries are the power source of choice for portable electronics.[1] Due to great advancements in battery chemistry, design, and manufacturing techniques, lithium-ion batteries are also being considered for space and automotive applications. Lithium-ion batteries promise significant weight savings over nickel–hydrogen batteries to power satellites. For hybrid electric and strictly electric vehicles, lithium-ion batteries are the leading candidate due to their high energy and power density, wide temperature range, long cycle life, and calendar life.

A major challenge for implementing lithium-ion batteries in applications such as satellite and electric vehicles is to ensure that they meet the demand for service life. Both applications require services of over 10 years and often involve heavy cycling. It is important to build a life model capable of accurately predicting life performance with limited accelerated testing. To establish a clear understanding of the life performance of a battery, it is necessary to understand its aging mechanisms. Such understanding needs to be acquired on cells of sufficient manufacturing maturity to ensure that the findings are relevant to the actual system performance. Moreover, batteries should be subjected to a variety of cycling and storage conditions to cover the range of scenarios anticipated during the product's life.

Lithium-ion batteries lose performance due to a loss of capacity and/or a rise in resistance.[2] Capacity loss is often associated with the loss of an active material. In a new lithium-ion battery, cell capacity is usually determined by the positive's capacity, which contains the total active lithium before operation. Upon use, lithium transports between the positive and the negative.[3] By design, the capacity of the negative (carbon) is usually not limiting because lithium plating could occur if the negative's capacity was smaller than that of the active lithium capacity. Increases in cell resistance can be attributed to many parts of the battery, including current collector corrosion and resistance of either the porous electrode or the electrolyte.[2]

Aging mechanism diagnosis is generally performed with a combination of electrochemical and structural physical analyses. Electrochemical techniques such as galvanostatic cycling at different rates, hybrid pulse power characterization (HPPC), and electrochemical impedance provide an assessment of low rate capacity loss and kinetic loss due to resistance increase.[2-15] From these analyses, it is often possible to deduce the source of degradation, for example, from the positive or the negative. Further elucidation of the mechanism may require postmortem physical analysis. Examples include structural analysis of the active materials by spectroscopic techniques such as X-ray diffraction (XRD) and Raman spectroscopy, morphological and microstructural characterization with scanning electron microscopy (SEM), and transmission electron microscopy.[4,7,16-25] In addition, IR spectroscopy has been a valuable tool in probing electrode surfaces, in particular, the solid electrolyte interface (SEI) layer known to exist on the negative.[26-29] Finally, electrochemical testing of the individual electrodes vs lithium metal often allows an assessment of the intrinsic capacity loss and/or resistance increase. However, issues with sampling location and changes in electrode compression compared to the original cell often cast doubt on the effectiveness of this technique. In contrast, it can be more advantageous to introduce a reference electrode that enables the monitoring of potentials of individual electrodes with minimum disturbance to the battery structure and operation.[30] Often, these diagnostic tools cannot pinpoint the exact processes that contribute to the cell aging. Eventually, assumptions that lead to models consistent with observations are necessarily made. For example, a parasitic reaction of the electrolyte decomposition can be postulated to account for lithium loss, even though direct evidence for the operation of this mechanism is often difficult to obtain.[31-35]

In this work, we apply various techniques mentioned above to the diagnosis of the commercial $LiFePO_4$/C cells manufactured by A123Systems. Earlier reports on laboratory-fabricated pouch cells of $LiFePO_4$/C cells concluded that no degradation of either the positive or the negative occurred as the cells aged, and active lithium loss was the main decay mechanism.[36] Our results are consistent with the lithium loss mechanism to be dominant for the commercial cell even though there appears to be large discrepancies in cycle life. Combined with our observations of the carbon negative, we postulate a mechanism based on the damage to the graphite SEI layer due to the intrinsic volume changes occurring during the cycling of the negative.

Experimental

The cells were acquired from A123Systems, Boston, MA. Details of the test matrix and testing protocols can be found elsewhere.[37] Briefly, cycling conditions covered temperatures of −30, 0, 15, 45, and 60°C, depth of discharges (DODs) of 10, 20, 50, 80, and 90%, and discharge rates of C/2, 2C, 6C, and 10C. The C rate is often used to express the rated capacity of a cell in terms of

* Electrochemical Society Active Member.
z E-mail: pliu@hrl.com

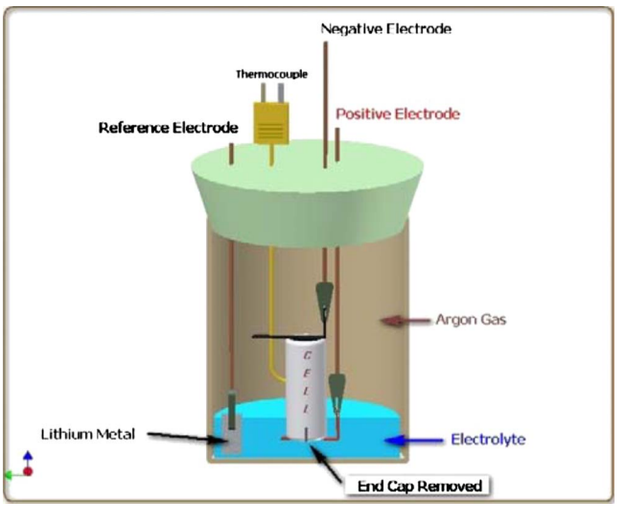

Figure 1. (Color online) Schematic of an in situ reference electrode measurement setup. The end cap of the cylindrical cell was removed. The cell is immersed in a liquid electrode, and a lithium reference electrode is located next to the cell. During constant current charge and discharge, the potential of the carbon negative can be recorded.

current. In our case, at a cell capacity near 2.2 Ah, the 1C rate is defined as the applied current of 2A. For the high rates, the testing matrix was chosen using a design of experiment program. Cells were either charged at a C/2 (for C/2 discharged cells) or at a 2C rate to a maximum voltage of 3.6 V, and a voltage hold was applied until the current was less than C/20 or 0.1 A. The end of discharge voltage of 2.0 V was used as a cutoff voltage as well as an end of life (EOL) criterion. Periodically, cells were taken off the cycling test and were subjected to several health diagnosis tests, including full capacity measurements at C/20, C/2, and 6C, ac impedance analysis (after 1 Ah of discharge from a fully charged state), and HPPC. Cycling tests were performed on either an Arbin BT-2400 system (Arbin Instruments, TX) or a Maccor battery testing system (Tulsa, OK). The ac impedance spectra [or electrochemical impedance spectroscopy (EIS)] were acquired with a Solartron electrochemical interface 1287 coupled with a Solartron frequency response analyzer 1260.

A setup was also designed to allow the in situ monitoring of individual electrode potentials during battery operation. The cell schematic is shown in Fig. 1. The end cap of the battery was removed to expose the end of the electrode jelly roll. This end was then immersed in a battery electrolyte of 1 M $LiPF_6$ in a 1:1 mixture of ethylene carbonate (EC)/dimethyl carbonate (DMC) from Kishida Chemical Co., Japan. A piece of lithium metal was placed in the electrolyte, which served as a reference electrode.

Selected EOL cells were disassembled after first being discharged to 2.0 V and were opened in a dry box filled with argon. Photographs of the electrodes and separators were taken during dismantling. The electrodes were sampled from three locations; approximately 3 cm wide sample pieces were taken from the beginning, the middle, and the end of the coil. The electrode samples for the electrochemical analysis were prepared by scraping the electrode material from one side of the current collector and by punching a disk with a total of six disks per electrode. The surface area of each electrode was 0.785 cm^2. Capacities of positive and negative electrodes were measured in Swagelok cells, where lithium metals were used as counter electrodes. All the Swagelok cell experiments in this paper are referring to a two-electrode Swagelok cell. The electrolyte solution was 1 M $LiPF_6$ in a 1:1 mixture of the EC/DMC mentioned previously. The carbon negative was briefly dipped in DMC to improve wetting by electrolyte. The half-cells were cycled at 6C, C/2, and C/20 rate.

The electrode samples for SEM, energy-dispersive X-ray analysis (EDX), and XRD were prepared by rinsing the surface in DMC. The electrolyte was extracted from one-third of the electrodes with 20 mL of DMC for electrolyte composition analysis by AA (Desert Analytics, Tuscon, AZ) to analyze Fe and Li contents. The SEM images and EDX were acquired on a Hitachi S-5400 system. XRD analysis was carried out on a Philips X'Pert system.

Results and Discussion

Cell resistance characterizations.— First, we show that the lithium iron phosphate battery ages primarily due to capacity loss rather than resistance increase. This finding is supported by observing the evolution of the discharge curves during the battery's life, the lack of impedance increase as measured by EIS, and the lack of resistance increase as measured by HPPC. For our discussion, unless otherwise mentioned, we primarily refer to the test results from the three cells cycled under the following conditions: A, 90% DOD, C/2, 15°C; B, 90% DOD, C/2, 60°C; and C, 50% DOD, 6C, 45°C.

Evolution of the discharge curves.— Figure 2 shows the discharge curves obtained at C/20 and C/2 after different numbers of cycles for cells A, B, and C. In all three cases, the shape of the discharge curves does not appreciably change as the cells age. The position of the plateau at ca. 3.3 V does not shift to lower voltages as the cells age, which suggests that cell resistance does not increase. Instead, the capacities measured at both C/20 and C/2 gradually decrease. This evolution of the cell discharge curve is distinctly different from what is commonly observed in lithium nickel cobalt aluminum oxide cells where resistance increases can dominate cell aging behavior.[7]

Electrochemical impedance.— Figure 3a shows the evolution of the Nyquist plots over the life of cell C. These results are consistent with the charge/discharge behavior, indicating that there is little evidence of impedance increase even when the cell reaches the EOL. Based on an analysis with an equivalent circuit commonly used for lithium-ion batteries (results not shown) that consists of a Randles circuit in series with an additional resistance–capacitor circuit in parallel (Fig. 3b),[38] our results indicate that there is a slight increase in the high frequency resistance and no change in the low frequency resistance, which correlates with charge transfer and solid-state diffusion of lithium ions. This observation is again in contrast with prior reported results on lithium nickel cobalt aluminum oxide cells where a large increase in resistance directly affects the battery aging.[5,39,40]

HPPC.— Figure 4 shows the potential and resistance profiles as a function of the state of charge (SOC) as cell C ages. No change in dc resistance measured with this technique is observed. The significant changes observed at high DODs (80 and 90%) are because of the apparent cell resistance increases when the battery approaches the end of discharge. The potential profiles also remain similar except for the reduced capacity as the cell ages. The position of the plateau remains the same at 3.3 V.

Charge–discharge curve analysis.— Under equilibrium conditions, lithium-ion battery cell capacities are often controlled by the amount of active lithium. Because metallic lithium plating is a major safety concern for lithium-ion batteries, excess carbon is used to ensure that it does not reach its capacity limit at the end of charging. During the charging step in the formation cycles, lithium ions are deintercalated from the positive and inserted into the carbon negative. Part of the lithium ions are being consumed for the construction of the SEI. Consequently, the amount of active lithium in the battery is less than either the negative or the positive capacities and directly determines the cell capacity. As the cells age, the cell capacity goes down according to the amount of the active lithium due to parasitic reactions in the battery, while the loss of positive or negative materials does not directly lead to capacity loss.

We analyzed the loss of active lithium through investigating the charge–discharge profiles, a method used previously with success in identifying battery capacity loss mechanisms.[41-43] This method re-

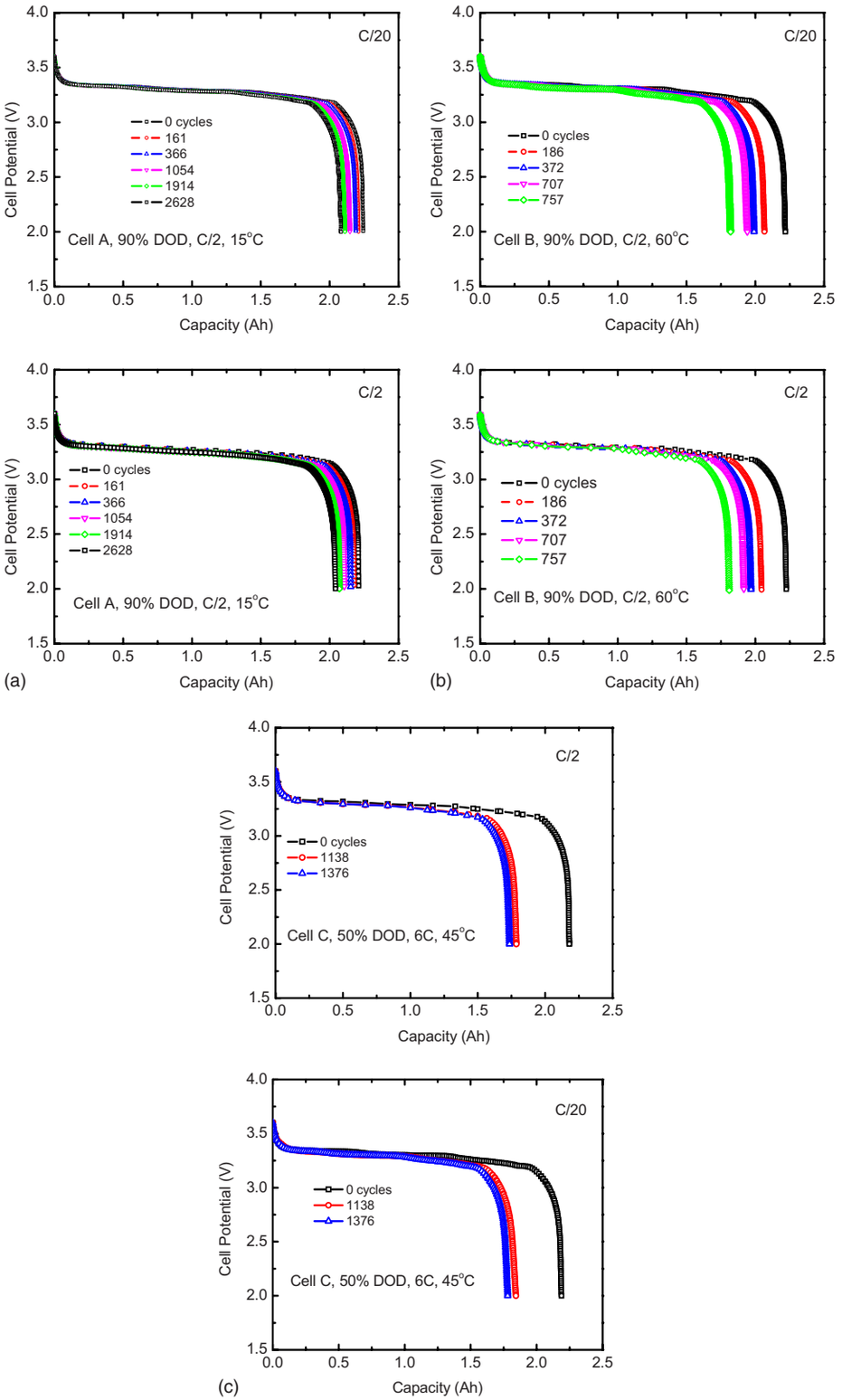

Figure 2. (Color online) C/2 and C/20 discharge profiles cycled at three different conditions denoted as cell A, 90% DOD, C/2, 15°C; cell B, 90% DOD, C/2, 60°C; and cell C: 50% DOD, 6C, 45°C.

lies on the unique features from the positive and negative reference profiles. Figure 5 shows charge profiles for the positive and the negative electrodes when measured against a lithium reference electrode, and their corresponding differentiation curves are shown in Fig. 6. The plateaus on the potential profile of the carbon negative correspond to the coexistence of lithiated graphite at different stages.[44,45] The dV/dSOC vs SOC curve shows three peaks that represent three distinct x values in Li_xC_6. The potential profile for $LiFePO_4$ has a single plateau that yields a featureless differentiation curve. Because the cell voltage equals the potential difference between the positive and the negative, the differentiation curve of the

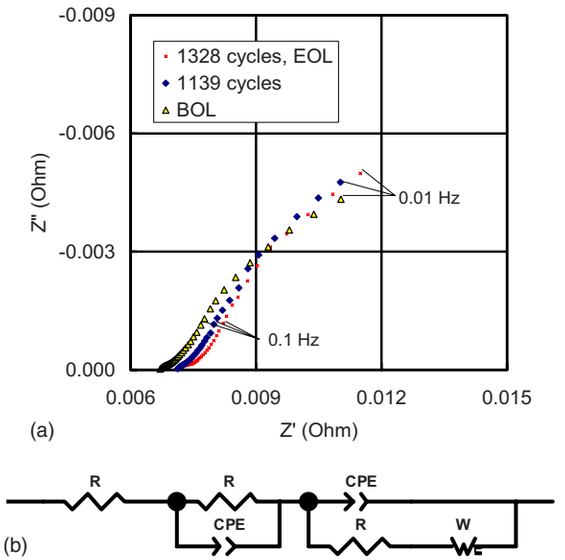

Figure 3. (Color online) (A) EIS spectra for cell C during its cycle life. There are 10 points for every decade change in frequency. The data points for 0.01 and 0.1 Hz are noted. (b) A schematic of the equivalent circuit, where R is resistor, CPE is constant phase element, and W is Warburg element.

cell only carries the features from the negative to the good approximation. By monitoring the movement of the peak positions on the curves, we can quantify the lithium concentration in the carbon negative.

Figure 7 shows the differentiation curves of cells A, B, and C. For cell A, three peaks observed from the battery cell corresponded very well with those of the negative profile (Fig. 6), confirming their graphite electrode origins. As the cell ages, all peaks move toward a lower DOD. The peaks shifting to the left indicate that the lithium content within the cell and available for discharge gradually decreases with cycling. The same trend is observed when analyzing the C/2 discharge curves, although the features are much less defined. Similar analyses were performed on cells B and C. We observe the same trend that indicates the reduction of active lithium in the negative at the beginning of cell discharge. This reduction is most likely due to the irreversible loss of active lithium. There is no evidence for residual active lithium in the positive at the end of charging because the cell voltage profile sharply rises, which represents the rise in positive voltage.

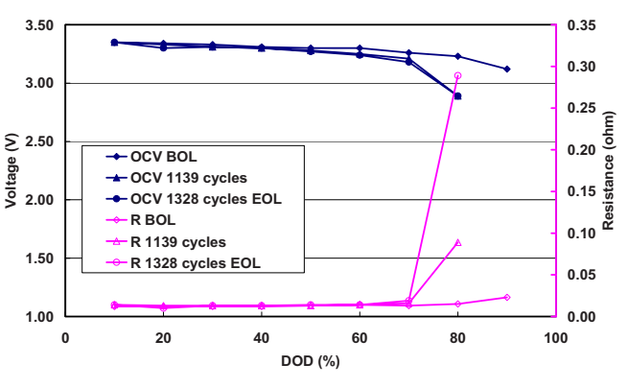

Figure 4. (Color online) Voltage and resistance as functions of DOD as calculated from HPPC test on cell C. There is no noticeable change during the battery's life except for the reduced capacity before reaching capacity depletion. DOD is defined with BOL capacity.

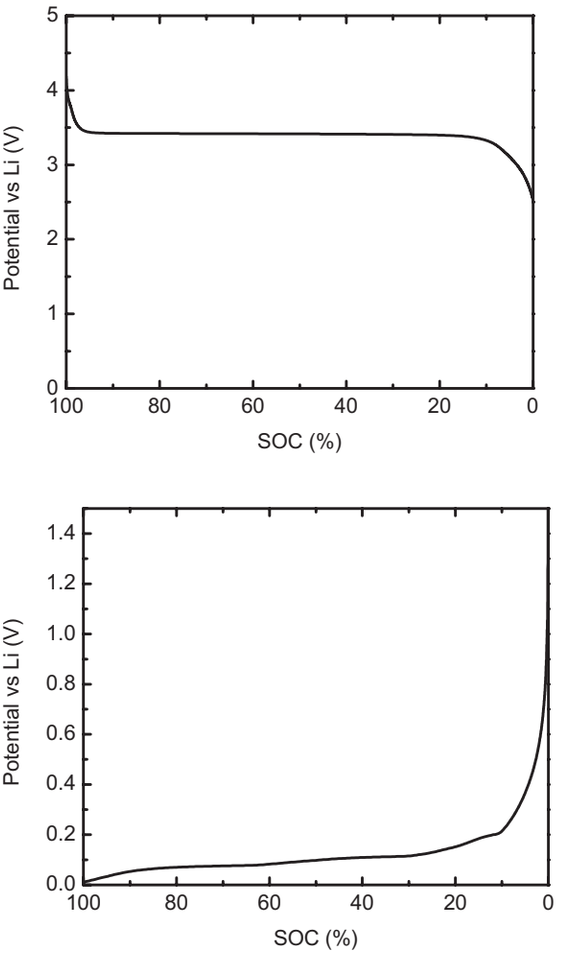

Figure 5. C/20 discharge curves for $LiFePO_4$ (top) and graphitic carbon (bottom) when measured against metal lithium.

Further analysis of the differentiation profiles for cells B and C also reveals the loss of an active negative material. Because the peak positions correspond to specific concentrations of lithium in carbon, the distance between any two peaks is necessarily proportional to the amount of active carbon because Δcapacity = mass of negative material $\times$ specific capacity $\times \Delta x$. As cell ages, reduction in the distance between the peaks represents the loss of negative materials. For example, at the beginning of the life of cell C, the distance between the first and the third peak is 1.167 Ah. By its EOL, the distance has decreased to 1.017 Ah. This reduction in negative capacity does not directly lead to capacity loss because there is always enough storage capacity for the amount of active lithium in the cell.

An alternative method of analyzing the charge–discharge profiles is based on plotting dQ (cell capacity)/dV vs V, which has been widely used.[4,44,46] This technique is also sensitive to cell performance decay as it clearly shows the potential regions where changes are taking place. Shown in Fig. 8 are the plots for cell B. The general features are consistent with those previously observed with graphite negative electrodes except for the extra feature at 3.25 V.[46] In the insert of Fig. 8, the dSOC/dV vs V plot for the negative electrode when measured against lithium metal is shown. All the features observed on the battery cell can clearly be attributed to the carbon negative including the extra feature. With cycling, the area under the peak at 3.34 V, which corresponds to the stage 1 lithium graphite compound, gradually decreases, which is consistent with the loss of active lithium. As active lithium is lost, the concentration

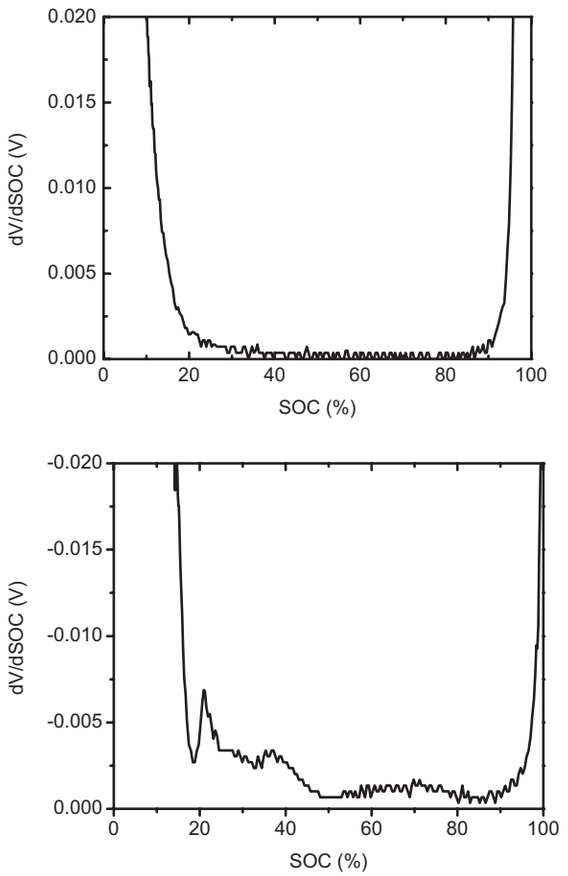

Figure 6. Differentiation curves for the discharge profiles shown in Fig. 4. The $LiFePO_4$ is essentially featureless.

of lithium in the carbon negative at the beginning of discharge decreases, which directly correlates with the reduction of the amount of stage 1 lithiated graphite, hence, the peak area at 3.34 V. The conclusion from the dQ/dV vs V analysis is thus consistent with that from the dV/dQ vs Q analysis.

To summarize, the shifting of the peaks on the dV/dQ vs Q voltage differentiation curves represents the total capacity loss (the active lithium loss), while the reduction in distance between the peaks represents the degradation of the carbon electrode and the associated loss in available sites for reaction with lithium. Both processes occur during cell aging, and we are able to estimate the losses based on the movement of the peaks. The results reveal that the amount of active lithium loss is higher than the amount of the negative material loss. These findings further underscore that lithium loss from the cell is responsible for the majority of the cell capacity fade.

In situ potential measurement.— The above postulated aging mechanism is further supported by our findings from in situ measurements performed with the setup described in Fig. 1. A fresh battery was cycled in this setup at 6C, 90% DOD, and 25°C. Its cycle life was comparable to that of a sealed cell, completing about 700 cycles before reaching EOL criteria. During C/2 and C/20 capacity characterization, the potential of the carbon negative was recorded vs the lithium reference electrode.

Figure 9 shows the evolution with cycling of the charge/discharge profile of the negative during a C/20 capacity characterization. During battery charging, the carbon negative shows a profile characteristic of that of graphitic carbon, with plateaus related to the formation of different staging compounds.[44,45] Two trends are worth noting. First, throughout the battery's life, the negative potential never reached 0 V vs Li/Li^+, indicating that the carbon negative was never fully intercalated; in other words, the amount of active lithium was always smaller than the capacity of the carbon negative. This in situ evidence provides direct support for our assertion that active lithium amount controls cell capacity. Second, with cycling and continuous loss of cell capacity, there is a reduction in the end of charge

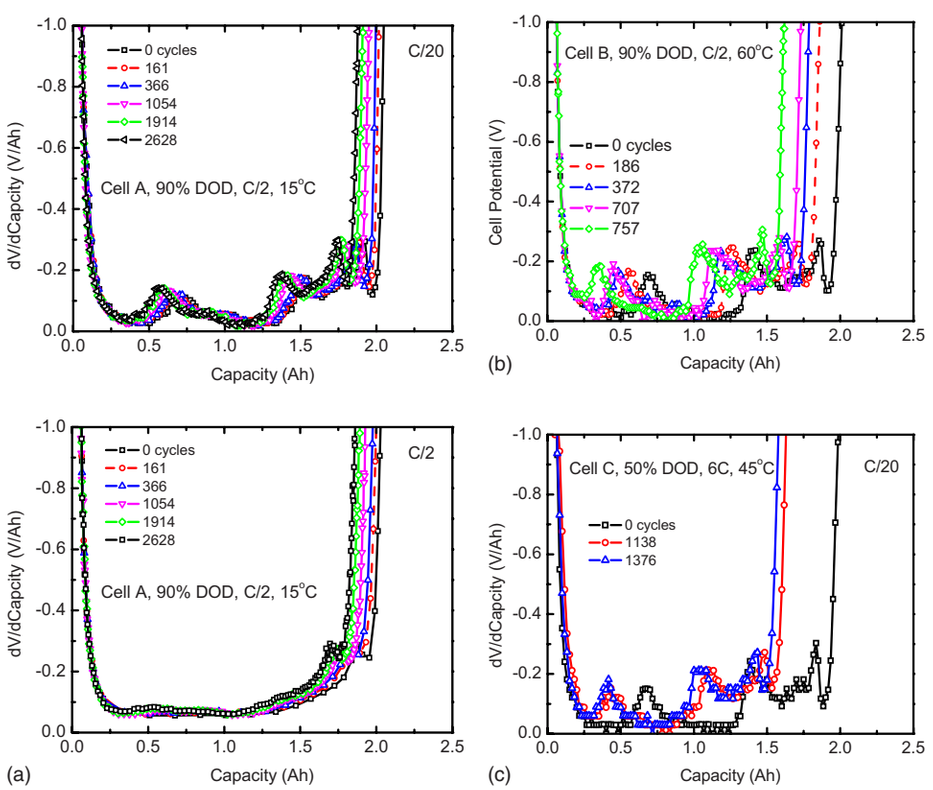

Figure 7. (Color online) Differentiation curves for cells A–C. The features are consistent with those from the graphitic carbon negative. As cycling progresses, all the features shift toward lower capacities. C/20 curves show much better resolution than the C/2 curves although the basic features are similar.

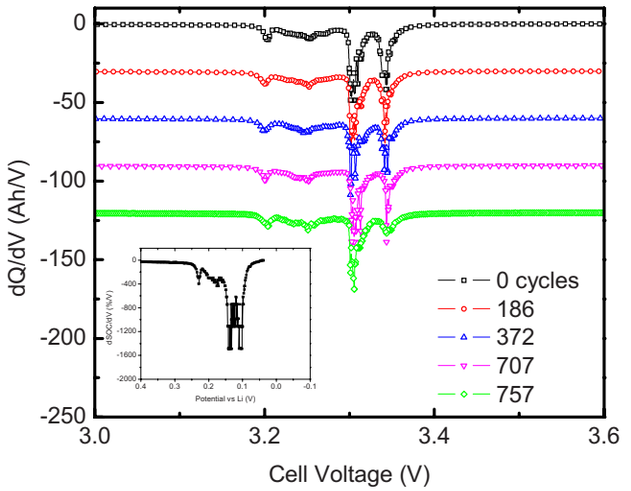

Figure 8. (Color online) dQ/dV vs V curves for cell B. The curves are vertically shifted for clarity. In the insert, the dSOC/dV vs V curve for the carbon negative when measured against lithium metal is shown (see Fig. 5).

voltage for the carbon negative (charge here means lithium insertion into carbon). This observation implies that lithium concentration in the available galleries of the graphite at the end of charge increases with cell capacity loss. If the cell only loses active lithium, the end concentration of lithium in carbon becomes lower and the end of charge potential becomes higher. The most likely reason for our observation is a loss of active carbon along with the loss of lithium. We can conclude that the in situ results agree very well with the electrochemical analysis discussed in the previous section.

Destructive physical analysis.— To further confirm the aging mechanisms, we have also performed destructive physical analysis, where selected cells were dismantled after they reached EOL. Figure 10 shows photographs of the negative and the positive during the cell disassembly of cell B. The surface of the positive electrode tape appears to be very smooth, and no visible change can be detected compared to a pristine cell. In contrast, the negative tape shows clear signs of delamination near the end of the tape. Tape delamination was observed on virtually all cells we disassembled.

SEM analysis was also carried out to investigate the surface morphologies of the disassembled cells. Figure 11 compares the images of the carbon negative from a beginning of life (BOL) cell, cell C,

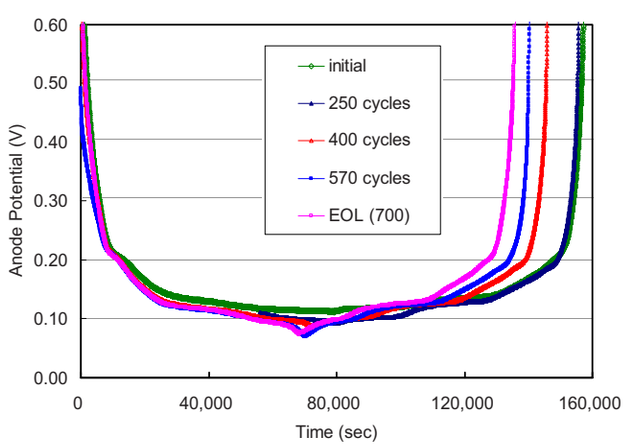

Figure 9. (Color online) Evolution of charge/discharge profiles of the carbon negative during the battery's life measured with a lithium reference electrode.

Figure 10. (Color online) Images of (bottom) negative and (top) positive tapes during destructive physical analysis of cell B. The positive tape appears to be pristine, while the negative tape shows clear signs of delamination near the edge of the tape.

and a cell that was cycled at 2C, 80% DOD, and 0°C. In the case of the 0°C cell, there is clear evidence of crack formation.

To examine the capacities of the electrodes, sections were punched out and tested in spring-loaded Swagelok cells against metallic lithium as the counter electrode. Figure 12 shows that both the positive and the negative appear to maintain all the capacities from the BOL, and there is no indication of resistance increase. This finding, when combined with the fact that the cell has lost 20% of its capacity, clearly demonstrates that loss of active lithium is the limiting mechanism for the full cell capacity loss. The fact that the carbon negative maintained capacity does not appear to contradict our earlier assertion that there is carbon loss from the negative. That is, first, carbon loss does not appear to be uniform across the dimension and length of the electrode tape with it being most severe near the edge of the tape and toward the center of the battery cell; second, the punched-out electrodes were tested in a spring- loaded Swagelok cell. Even if there is carbon delamination, the compression force applied by the spring might reconnect the delaminated carbon to the copper current collector. As long as the storage capacity of the carbon anode did not degrade, its full capacity can be accessed.

Loss of active lithium due to parasitic reactions in lithium-ion batteries is a widely known phenomenon and is often the dominant concern for cell calendar life.[3] It is most likely associated with the carbon negative. Lithiated carbon only functions as an effective negative material due to the existence of the SEI layer on its surface.

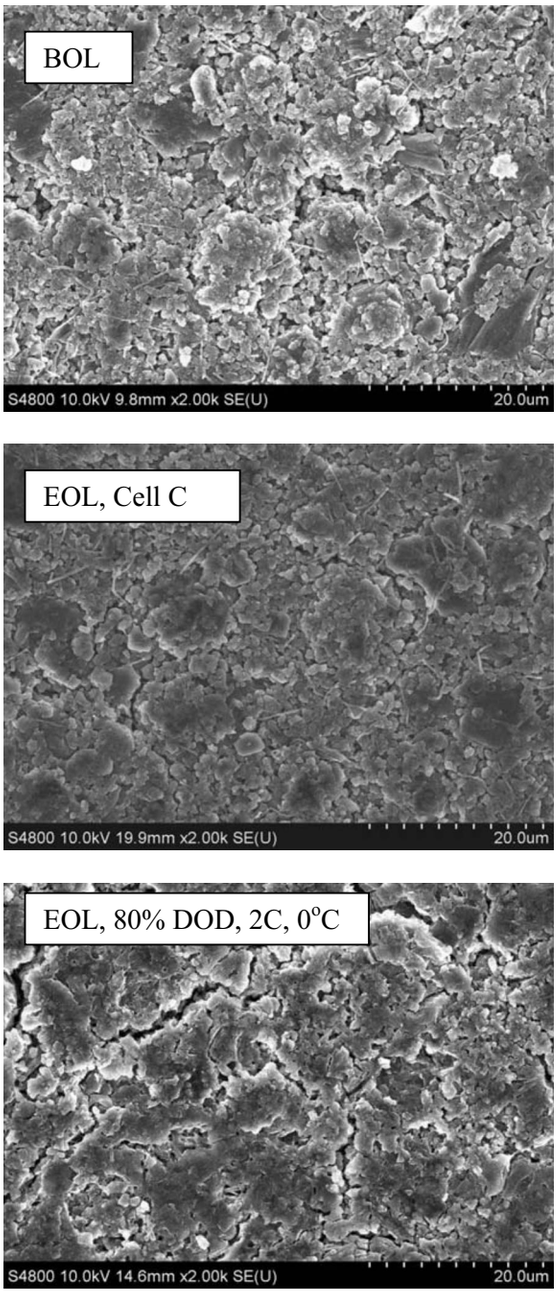

Figure 11. SEM images of the negatives extracted from an as-received cell, cell C at EOL, and a cell cycled at 80% DOD, 2C, 0°C, which showed the most pronounced microcracks.

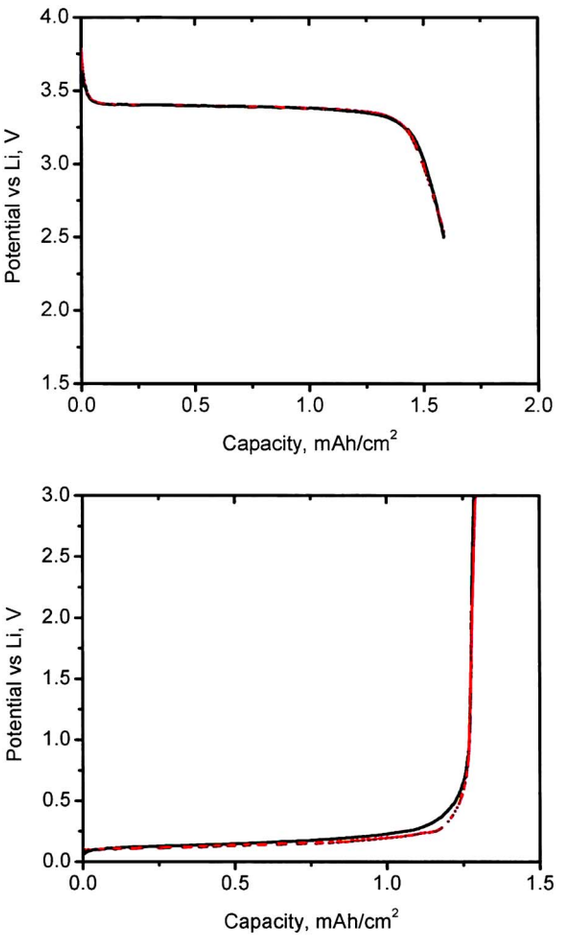

Figure 12. (Color online) Discharge profiles (red dotted line) of positive (top) and negative (bottom) extracted from cell C when discharged against lithium compared to those from an as-received cell (black lines). No apparent change is observed.

It is suggested that the SEI layer is an electronic insulator but an ion conductor. The protective layer prevents a substantial reaction between the low voltage negative and the organic electrolyte. As a result, the stability of the SEI layer is of paramount importance to the life of lithium-ion batteries.

Lithium-ion batteries can lose capacity when active lithium is consumed to construct and repair the SEI layer. During cell storage, continuous growth of or electric leakage through the layer can lead to persistent capacity loss. Moreover, any perturbations to the SEI layer either due to chemical or mechanical forces likely accelerate lithium loss. In spinel $LiMn_2O_4$ batteries, it is established that the dissolved Mn transports to the negative where it is reduced, thereby increasing the conductivity of the SEI layer.[47-49] Any electronic conduction through the SEI layer promotes additional parasitic electrochemical reaction to passivate the conducting surface. Similar concerns exist for $LiFePO_4$ cells because Fe from the positive can dissolve into the electrolyte and migrate to the negative.[50] Therefore, we further investigated the Fe dissolution of $LiFePO_4$ through elemental analysis using atomic absorbance spectrophotometry. We analyzed the electrolyte extracted from EOL cells. The BOL cell electrolyte shows an Fe/Li ratio of 0.0013. Assuming a Li concentration of 1 M, the Fe concentration is 1.3 mM. In comparison, cell C at the EOL has an Fe concentration of 1.5 mM. Because cell C was cycled at 45°C, a slight increase in Fe dissolution is expected. However, the overall level is very low and does not represent a major issue. Moreover, the surface of the negative was analyzed by EDX; only carbon, oxygen, and fluorine were detected, and no Fe was observed within our detection limit. We can conclude that Fe dissolution is not likely a concern for these cells, which is also consistent with the lack of capacity degradation from the positive.

Having excluded the chemical instability of the SEI layer due to Fe dissolution, its mechanical stability becomes our main interest. Figure 11 shows that both the positive and the negative of cell C appear to maintain all the capacities from the BOL, and there is no indication of resistance increase. To maintain a stable SEI layer, the carbon negative needs to be dimensionally stable. However, graphitic carbon negative can experience a $>10\%$ change in volume during battery cycling.[51] The SEI layer must accommodate this same volume change. If the SEI layer is not elastic enough, any

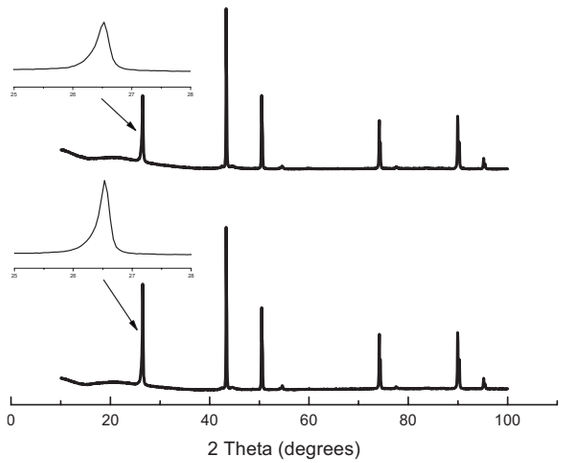

Figure 13. XRD diagrams of negative from an as-received cell (bottom) and cell C. The first peak, which is the 002 diffraction from graphite, was expanded to show the broadening after cycling.

breakage exposes a fresh surface of carbon negative, which needs to be passivated with the consumption of active lithium (and electrolyte species). The batteries in the current study have shown clear signs of negative instability. As discussed above, there is a loss of active carbon from the batteries, which is likely to be electrically isolated from the current collector. In addition, the physical appearance shown in Fig. 10 and 11 indicates cracking and delamination of the carbon layer from the current collector. Tape delamination was not observed on fresh cells. Physical changes in the carbon negative also take place at the particle level. Figure 13 compares the XRD patterns of carbon negatives extracted from as-made cells and cell C at EOL. The general patterns do not change appreciably from the BOL and are consistent with those of crystalline graphite. However, a comparison of the 002 peaks at 26.5° shows that cycling has induced a broadening of this peak. Crystallite size was estimated using the Scherrer fomula based on the full width at half-maximum values. The results showed that the crystallite size has decreased from 0.33 to 0.12 μm after cycling. Because the 002 peak measures the long-range ordering on the direction perpendicular to the graphene sheets, the reduction in crystallites indicates that graphite exfoliation has occurred during the battery's life.

Based on both electrochemical and structural analyses, we propose the following mechanism to account for the capacity loss of $LiFePO_4$ cells. The capacities of these batteries are controlled by the amount of active lithium. Consequently, the capacity loss is directly related to the loss of active lithium. The instability of the carbon negative/electrolyte interface is suspected to be the source of the lithium loss. The volume change during battery cycling introduces irreversible damage to the SEI layer whose subsequent repair consumes active lithium. The change in the carbon negative is apparent both at the crystal structure scale, as evidenced by exfoliation, and at the macroscale, as shown by crack formation and delamination from the current collector. This mechanism serves as the foundation for a semiempirical life model that is reported elsewhere.[52]

Conclusions

The graphite/iron phosphate batteries in this study do not experience appreciable resistance increase under a variety of cycling conditions. Instead, the batteries lose their capacities as they cycle. The capacities of these cells are limited not by the storage capacities of the negative or the positive but rather by the amount of active lithium. As a result, loss of active lithium is the dominating mechanism responsible for cell capacity loss. An analysis of the discharge profiles reveals the loss of active lithium as well as loss of carbon. A destructive physical analysis of the cycled cells shows physical degradation of the carbon negative. In addition, XRD diagrams reveal the exfoliation of the graphite layers during long-term cycling. We propose that the instability of the negative results in the instability of the SEI layer whose repair greatly accelerates losses of active lithium and cell capacity.

HRL Laboratories assisted in meeting the publication costs of this article.

References

1. J. M. Tarascon and M. Armand, *Nature (London)*, **414**, 359 (2001).
2. J. Vetter, P. Novak, M. R. Wagner, C. Veit, K. C. Moller, J. O. Besenhard, M. Winter, M. Wohlfahrt-Mehrens, C. Vogler, and A. Hammouche, *J. Power Sources*, **147**, 269 (2005).
3. J. Christensen and J. Newman, *J. Electrochem. Soc.*, **152**, A818 (2005).
4. K. A. Striebel, J. Shim, E. J. Cairns, R. Kostecki, Y. J. Lee, J. Reimer, T. J. Richardson, P. N. Ross, X. Song, and G. V. Zhuang, *J. Electrochem. Soc.*, **151**, A857 (2004).
5. M. Broussely, S. Herreyre, P. Biensan, P. Kasztejna, K. Nechev, and R. J. Staniewicz, *J. Power Sources*, **97–98**, 13 (2001).
6. L. J. Hardwick, M. Marcinek, L. Beer, J. B. Kerr, and R. Kostecki, *J. Electrochem. Soc.*, **155**, A442 (2008).
7. R. Kostecki, J. L. Lei, F. McLarnon, J. Shim, and K. Striebel, *J. Electrochem. Soc.*, **153**, A669 (2006).
8. K. Kumaresan, Q. Z. Guo, P. Ramadass, and R. E. White, *J. Power Sources*, **158**, 679 (2006).
9. B. Y. Liaw, E. P. Roth, R. G. Jungst, G. Nagasubramanian, H. L. Case, and D. H. Doughty, *J. Power Sources*, **119–121**, 874 (2003).
10. E. Markervich, G. Salitra, M. D. Levi, and D. Aurbach, *J. Power Sources*, **146**, 146 (2005).
11. R. P. Ramasamy, J. W. Lee, and B. N. Popov, *J. Power Sources*, **166**, 266 (2007).
12. R. P. Ramasamy, R. E. White, and B. N. Popov, *J. Power Sources*, **141**, 298 (2005).
13. G. Sarre, P. Blanchard, and M. Broussely, *J. Power Sources*, **127**, 65 (2004).
14. M. Wohlfahrt-Mehrens, C. Vogler, and J. Garche, *J. Power Sources*, **127**, 58 (2004).
15. T. Yoshida, M. Takahashi, S. Morikawa, C. Ihara, H. Katsukawa, T. Shiratsuchi, and J. Yamaki, *J. Electrochem. Soc.*, **153**, A576 (2006).
16. D. P. Abraham, R. D. Twesten, M. Balasubramanian, J. Kropf, D. Fischer, J. McBreen, I. Petrov, and K. Amine, *J. Electrochem. Soc.*, **150**, A1450 (2003).
17. A. M. Andersson, D. P. Abraham, R. Haasch, S. MacLaren, J. Liu, and K. Amine, *J. Electrochem. Soc.*, **149**, A1358 (2002).
18. M. Balasubramanian, H. S. Lee, X. Sun, X. Q. Yang, A. R. Moodenbaugh, J. McBreen, D. A. Fischer, and Z. Fu, *Electrochem. Solid-State Lett.*, **5**, A22 (2002).
19. K. Y. Chung, H. S. Lee, W. S. Yoon, J. McBreen, and X. Q. Yang, *J. Electrochem. Soc.*, **153**, A774 (2006).
20. M. Kerlau, M. Marcinek, V. Srinivasan, and R. M. Kostecki, *Electrochim. Acta*, **52**, 5422 (2007).
21. R. Kostecki and F. McLarnon, *J. Power Sources*, **119–121**, 550 (2003).
22. R. Kostecki and F. McLarnon, *Electrochem. Solid-State Lett.*, **7**, A380 (2004).
23. H. H. Li, N. Yabuuchi, Y. S. Meng, S. Kumar, J. Breger, C. P. Grey, and Y. Shao-Horn, *Chem. Mater.*, **19**, 2551 (2007).
24. N. Yabuuchi, Y. T. Kim, H. H. Li, and Y. Shao-Horn, *Chem. Mater.*, **20**, 4936 (2008).
25. N. Yabuuchi, S. Kumar, H. H. Li, Y. T. Kim, and Y. Shao-Horn, *J. Electrochem. Soc.*, **154**, A566 (2007).
26. D. Aurbach, *J. Power Sources*, **119–121**, 497 (2003).
27. D. Aurbach, B. Markovsky, G. Salitra, E. Markevich, Y. Talyossef, M. Koltypin, L. Nazar, B. Ellis, and D. Kovacheva, *J. Power Sources*, **165**, 491 (2007).
28. D. Aurbach, Y. Talyosef, B. Markovsky, E. Markevich, E. Zinigrad, L. Asraf, J. S. Gnanaraj, and H. J. Kim, *Electrochim. Acta*, **50**, 247 (2004).
29. M. Koltypin, D. Aurbach, L. Nazar, and B. Ellis, *Electrochem. Solid-State Lett.*, **10**, A40 (2007).
30. Y. Zhang and C. Y. Wang, *J. Electrochem. Soc.*, **156**, A527 (2009).
31. D. Aurbach, *J. Power Sources*, **89**, 206 (2000).
32. D. Aurbach, E. Zinigrad, Y. Cohen, and H. Teller, *Solid State Ionics*, **148**, 405 (2002).
33. R. Darling and J. Newman, *J. Electrochem. Soc.*, **145**, 990 (1998).
34. G. Ning and B. N. Popov, *J. Electrochem. Soc.*, **151**, A1584 (2004).
35. G. Ning, R. E. White, and B. N. Popov, *Electrochim. Acta*, **51**, 2012 (2006).
36. K. Striebel, J. Shim, A. Sierra, H. Yang, X. Y. Song, R. Kostecki, and K. McCarthy, *J. Power Sources*, **146**, 33 (2005).
37. J. Hicks-Garner, J. Wang, W. Li, E. Sherman, S. Soukiazian, and P. Liu, Unpublished work.
38. S. R. Narayanan, D. H. Shen, S. Surampudi, A. I. Attia, and G. Halpert, *J. Electrochem. Soc.*, **140**, 1854 (1993).
39. I. Bloom, S. A. Jones, E. G. Polzin, V. S. Battaglia, G. L. Henriksen, C. G. Motloch, R. B. Wright, R. G. Jungst, H. L. Case, and D. H. Doughty, *J. Power Sources*, **111**, 152 (2002).
40. R. B. Wright, C. G. Motloch, J. R. Belt, J. P. Christophersen, C. D. Ho, R. A. Richardson, I. Bloom, S. A. Jones, V. S. Battaglia, G. L. Henriksen, et al., *J. Power Sources*, **110**, 445 (2002).
41. I. Bloom, J. Christophersen, and K. Gering, *J. Power Sources*, **139**, 304 (2005).
42. I. Bloom, J. P. Christophersen, D. P. Abraham, and K. L. Gering, *J. Power Sources*, **157**, 537 (2006).

43. I. Bloom, A. N. Jansen, D. P. Abraham, J. Knuth, S. A. Jones, V. S. Battaglia, and G. L. Henriksen, *J. Power Sources*, **139**, 295 (2005).
44. M. W. Verbrugge and B. J. Koch, *J. Electrochem. Soc.*, **150**, A374 (2003).
45. M. Winter, J. O. Besenhard, M. E. Spahr, and P. Novak, *Adv. Mater.*, **10**, 725 (1998).
46. S. Megahed and B. Scrosati, *J. Power Sources*, **51**, 79 (1994).
47. A. Blyr, C. Sigala, G. Amatucci, D. Guyomard, Y. Chabre, and J. M. Tarascon, *J. Electrochem. Soc.*, **145**, 194 (1998).
48. N. Kumagai, S. Komaba, Y. Kataoka, and M. Koyanagi, *Chem. Lett.*, **29**, 1154 (2000).
49. H. Tsunekawa, S. Tanimoto, R. Marubayashi, M. Fujita, K. Kifune, and M. Sano, *J. Electrochem. Soc.*, **149**, A1326 (2002).
50. K. Amine, J. Liu, and I. Belharouak, *Electrochem. Commun.*, **7**, 669 (2005).
51. R. Yazami and Y. Reynier, *J. Power Sources*, **153**, 312 (2006).
52. J. Wang, P. Liu, J. Hicks-Garner, W. Li, E. Sherman, and S. Soukiazian, Report, HRL Laboratories, LLC, Malibu, CA (2009).